# Dynamic absorption and scattering of water and hydrogel during high-repetition-rate (>100 MHz) burst-mode ultrafast-pulse laser ablation

**Zuoming Qian,[1] Andrés Covarrubias,[1] Alexander W. Grindal,[1] Margarete K. Akens,[2,3] Lothar Lilge,[3,4] and Robin S. Marjoribanks[1,*]**

[1]*Department of Physics, University of Toronto, 60 St. George Street, Toronto, Ontario, M5S 1A7, Canada*
[2]*Techna Institute, University Health Network, 100 College Street, Toronto, Ontario, M5G 1P5, Canada*
[3]*Department of Medical Biophysics, University of Toronto, 101 College Street, Toronto, Ontario, M5G 1L7, Canada*
[4]*Princess Margaret Cancer Centre, 101 College Street, Toronto, Ontario, M5G 1L7, Canada*
[*]*marj@physics.utoronto.ca*

**Abstract**: High-repetition-rate burst-mode ultrafast-laser ablation and disruption of biological tissues depends on interaction of each pulse with the sample, but under those particular conditions which persist from previous pulses. This work characterizes and compares the dynamics of absorption and scattering of a 133-MHz repetition-rate, burst-mode ultrafast-pulse laser, in agar hydrogel targets and distilled water. The differences in energy partition are quantified, pulse-by-pulse, using a time-resolving integrating-sphere-based device. These measurements reveal that high-repetition-rate burst-mode ultrafast-laser ablation is a highly dynamical process affected by the persistence of ionization, dissipation of plasma plume, neutral material flow, tissue tensile strength, and the hydrodynamic oscillation of cavitation bubbles.

**OCIS codes**: (140.7090) Ultrafast lasers; (170.1020) Ablation of tissue; (160.1435) Biomaterials.

## References and links

1. S. H. Chung and E. Mazur, "Surgical applications of femtosecond lasers," J. Biophotonics **2**(10), 557–572 (2009).
2. R. R. Gattass and E. Mazur, "Femtosecond laser micromachining in transparent materials," Nat. Photonics **2**(4), 219–225 (2008).
3. R. S. Marjoribanks, C. Dille, J. E. Schoenly, L. McKinney, A. Mordovanakis, P. Kaifosh, P. Forrester, Z. Qian, A. Covarrubias, Y. Feng, and L. Lilge, "Ablation and thermal effects in treatment of hard and soft materials and biotissues using ultrafast-laser pulse-train bursts," Photonics Lasers Med. **1**(3), 155 (2012).
4. C. L. Hoy, O. Ferhanoglu, M. Yildirim, S. S. Karajanagi, K. M. C. Chan, J. B. Kobler, S. M. Zeitels, and A. Ben-Yakar, "Clinical ultrafast laser surgery: recent advances and future directions," IEEE J. Sel. Top. Quantum Electron. **20**(2), 242–255 (2014).
5. A. Vogel and V. Venugopalan, "Mechanisms of Pulsed Laser Ablation of Biological Tissues (Chem. Rev.2003, 103, 577−644. Published on the Web 02/12/03.)," Chem. Rev. **103**(5), 2079 (2003).
6. A. Vogel, J. Noack, G. Hüttman, and G. Paltauf, "Mechanisms of femtosecond laser nanosurgery of cells and tissues," Appl. Phys. B **81**(8), 1015–1047 (2005).
7. F. Docchio, "Lifetimes of Plasmas Induced in Liquids and Ocular Media by Single Nd:YAG Laser Pulses of Different Duration," Europhys. Lett. **6**(5), 407–412 (1988).
8. I. Apitz and A. Vogel, "Material ejection in nanosecond Er:YAG laser ablation of water, liver, and skin," Appl. Phys., A Mater. Sci. Process. **81**(2), 329–338 (2005).
9. A. Vogel and V. Venugopalan, "Pulsed Laser Ablation of Soft Biological Tissues," in *Optical-Thermal Response of Laser-Irradiated Tissue*, A. J. Welch and M. J. C. van Gemert, eds. 2nd ed. (Springer Science + Business Media B. V., 2011), pp. 551–615.
10. P. R. Herman, A. Oettl, K. P. Chen, and R. S. Marjoribanks, "Laser micromachining of transparent fused silica with 1-ps pulses and pulse trains," Proc. SPIE **3616**, 148–155 (1999).
11. S. Eaton, H. Zhang, P. Herman, F. Yoshino, L. Shah, J. Bovatsek, and A. Arai, "Heat accumulation effects in femtosecond laser-written waveguides with variable repetition rate," Opt. Express **13**(12), 4708–4716 (2005).
12. L. Ding, R. Blackwell, J. F. Künzler, and W. H. Knox, "Large refractive index change in silicone-based and non-

silicone-based hydrogel polymers induced by femtosecond laser micro-machining," Opt. Express **14**(24), 11901–11909 (2006).

13. D. E. Savage, D. R. Brooks, M. DeMagistris, L. Xu, S. MacRae, J. D. Ellis, W. H. Knox, and K. R. Huxlin, "First demonstration of ocular refractive change using blue-IRIS in live cats," Invest. Ophthalmol. Vis. Sci. **55**(7), 4603–4612 (2014).
14. A. Vogel, J. Noack, K. Nahen, D. Theisen, S. Busch, U. Parlitz, D. X. Hammer, G. D. Noojin, B. A. Rockwell, and R. Birngruber, "Energy balance of optical breakdown in water at nanosecond to femtosecond time scales," Appl. Phys. B **68**(2), 271–280 (1999).
15. Z. Qian, J. E. Schoenly, A. Covarrubias, L. Lilge, and R. S. Marjoribanks, "Energy-partition diagnostic for measuring time-resolved scattering and absorption in burst-mode laser ablation," Rev. Sci. Instrum. **85**(3), 033101 (2014).
16. A. Vogel, K. Nahen, D. Theisen, and J. Noack, "Plasma formation in water by picosecond and nanosecond Nd: YAG laser pulses. I. Optical breakdown at threshold and superthreshold irradiance," IEEE J. Sel. Top. Quantum Electron. **2**(4), 847–860 (1996).
17. K. Nahen and A. Vogel, "Plasma formation in water by picosecond and nanosecond Nd: YAG laser pulses. II. Transmission, scattering, and reflection," IEEE J. Sel. Top. Quantum Electron. **2**(4), 861–871 (1996).
18. Z. Qian, A. Mordovanakis, J. E. Schoenly, A. Covarrubias, Y. Feng, L. Lilge, and R. S. Marjoribanks, "Pulsetrain-burst mode, ultrafast-laser interactions with 3D viable cell cultures as a model for soft biological tissues," Biomed. Opt. Express **5**(1), 208–222 (2014).
19. A. Vogel, M. R. Capon, M. N. Asiyo-Vogel, and R. Birngruber, "Intraocular photodisruption with picosecond and nanosecond laser pulses: tissue effects in cornea, lens, and retina," Invest. Ophthalmol. Vis. Sci. **35**(7), 3032–3044 (1994).
20. T. Juhasz and G. Kastis, "Shock wave and cavitation bubble dynamics during photodisruption in ocular media and their dependence on the pulse duration," Proc. SPIE **2681**, 428–436 (1996).
21. E. A. Brujan, K. Nahen, P. Schmidt, and A. Vogel, "Dynamics of laser-induced cavitation bubbles near an elastic boundary," J. Fluid Mech. **433**, 251–281 (2001).
22. N. Tinne, E. Lübking, H. Lubatschowski, A. Krüger, and T. Ripken, "The influence of a spatial and temporal pulse-overlap on the laser-tissue-interaction of modern ophthalmic laser systems," Biomed. Tech. (Berl.) **57**(SI-1 Track-P Suppl 1), 4115 (2012).
23. D. von der Linde and H. Schüler, "Breakdown threshold and plasma formation in femtosecond laser–solid interaction," J. Opt. Soc. Am. B **13**(1), 216–222 (1996).
24. R. Röttgers, D. McKee, and C. Utschig, "Temperature and salinity correction coefficients for light absorption by water in the visible to infrared spectral region," Opt. Express **22**(21), 25093–25108 (2014).
25. C. Kerse, H. Kalaycıoğlu, P. Elahi, Ö. Akçaalan, and F. Ö. Ilday, "3.5-GHz intra-burst repetition rate ultrafast Yb-doped fiber laser," Opt. Commun. **366**, 404–409 (2016).
26. C. Kerse, "Ablation cooled material removal with bursts of ultrafast pulses," Bilkent University (2016).
27. I. Akhatov, O. Lindau, A. Topolnikov, R. Mettin, N. Vakhitova, and W. Lauterborn, "Collapse and rebound of a laser-induced cavitation bubble," Phys. Fluids **13**(10), 2805–2819 (2001).
28. E. A. Brujan and A. Vogel, "Stress wave emission and cavitation bubble dynamics by nanosecond optical breakdown in a tissue phantom," J. Fluid Mech. **558**, 281 (2006).
29. W. Lauterborn and A. Vogel, *Bubble Dynamics and Shock Waves* (Springer Berlin Heidelberg, 2013), pp. 67–103.
30. R. C. C. Chen, Y. T. Yu, K. W. Su, J. F. Chen, and Y. F. Chen, "Exploration of water jet generated by Q-switched laser induced water breakdown with different depths beneath a flat free surface," Opt. Express **21**(1), 445–453 (2013).
31. J. R. Blake and D. C. Gibson, "Cavitation bubbles near boundaries," Annu. Rev. Fluid Mech. **19**(1), 99–123 (1987).
32. R. H. Cole and R. Weller, "Underwater explosions," Phys. Today **1**(6), 35 (1948).
33. A. Vogel, S. Busch, and U. Parlitz, "Shock wave emission and cavitation bubble generation by picosecond and nanosecond optical breakdown in water," J. Acoust. Soc. Am. **100**(1), 148–165 (1996).

## 1. Introduction

Ultrashort-pulse lasers have proven themselves indispensable as tools of today's industrial materials-processing, and have already come to dominate niche applications in ophthalmology and other clinical applications in medicine, including corneal dissection in IntraLASIK refractive-correction surgery, and femtosecond laser-assisted cataract surgery [1]. Ultrafast lasers provide refinement in control together with smoother and cleaner cuts, with less histological insult than nanosecond or longer pulsed lasers [2]. There are strong and ongoing efforts [1–3] devoted to expanding the applications of ultrafast lasers to other areas of medicine, such as dentistry, dermatology, and cardiology [4].

In ultrafast-laser ablation at an interface, when pulse irradiance reaches a material-specific 'dielectric-breakdown threshold', the ultrafast pulse ionizes the target material and creates a

plasma at the laser focus [5]. The several-hundred-nanometers thick layer of heated material created during the very brief irradiation rapidly decouples from the bulk material and is driven away by the high pressure-gradient across the thin heated layer, allowing the substrate material to remain relatively cool. It is this decoupling mechanism that halts thermal diffusion into the tissue, leading to the low collateral damage characteristic of ultrafast laser ablation as compared to ablation performed by longer-pulse counterparts [3,5,6].

Most current microjoule-level commercial ultrafast laser systems deliver pulses at kilohertz, or hundreds of kilohertz repetition rate. For laser systems operating at kilohertz repetition-rate, the physics of ablation by each pulse is mostly isolated from the effects of other pulses: At this repetition rate, pulses are separated by tens of microseconds; therefore, when any subsequent pulse arrives, the target material has cooled down, and the plasma created by previous pulses has already dissipated [7].

However, when the pulses are applied at megahertz repetition rate and in particular above 100 MHz repetition rate, new physics mechanisms begin to emerge due to pulse-to-pulse dynamics, wherein a later pulse can interact with the plasma or the plume of ejected material created by the previous pulses [8,9]. Additionally, heat left behind by proceeding pulses, while insignificant at lower repetition rates, starts to accumulate significantly at high repetition-rates. In other words, the target material, by being physically modified, still retains "memory" of previous pulses, which in turn affects the interaction between the material and subsequent pulses, thus influencing the final ablation results [3].

This "memory" timescale, relevant for high-repetition-rate irradiation, has been exploited in materials-processing applications, and has shown strong potential in novel ultrafast-laser surgery applications currently under development. High-repetition-rate pulsetrain-burst-mode ultrafast lasers are shown to mitigate the micro-cracking noted in laser ablation of brittle materials [10]. In materials-processing applications, continuous-running high-repetition-rate ultrafast lasers have been successfully applied to refractive index changes in glass and ophthalmologic hydrogel polymers [11,12]. For the development of surgical applications, high-repetition-rate ultrafast lasers are being evaluated for the next-generation refraction-correction laser surgery known as 'intra-tissue refractive index shaping (IRIS)'. [13] Rather than modifying the cornea's figure (as in LASIK), IRIS is a procedure that corrects a patient's focusing ability by altering the optical power of the cornea through modifying the refractive index of it via the heat-accumulation effect of high-repetition-rate ultrafast lasers [13]. Overall, high-repetition-rate ultrafast lasers are becoming an increasingly important class of lasers in both materials processing and surgical applications.

Among high-repetition-rate ultrafast lasers, pulsetrain-burst-mode lasers have shown great promise as platforms for future laser surgery, because they offer additional routes of control via their pulsetrain-burst duration, pulsetrain repetition rate, and even by shaping the pulsetrain envelope, while retaining the characteristic precision and efficiency of high-reception-rate ultrafast lasers. With this expanded parameter-space, burst-mode lasers provide greater flexibility in tailoring the laser effect to meet specific surgical needs, according to the optical and mechanical properties of different target tissues.

To utilize fully these extra control options, it is essential to understand the dynamics of pulse-to-pulse interaction, mediated by the material during the burst-mode ablation. Considering that all physical phenomena in plasma-mediated ablation (*i.e.* cavitation, shock-wave propagation, heat diffusion, material ejection and ablation plume formation) depend on the energy absorbed by the target during each pulse [14], pulse-by-pulse characterization of absorption throughout the pulsetrain is the centerpiece in the investigation of the burst-mode ablation mechanisms.

To characterize absorption during burst-mode laser ablation at a free surface, pulse-by-pulse time resolution is required. For this purpose, we designed, built and demonstrated the use of an energy-partition diagnostic device in a previous work [15].

In this paper we report our findings to characterize the absorption dynamics at the air interface with water and hydrogels of different concentrations as a model for surface ablation of soft tissues with various weak tensile strengths during high-repetition-rate burst-mode ablation. Water and agar gel provide similar laser-induced optical-breakdown threshold as ocular media [16,17]. Water and agar-gel targets are optically transparent, and are easy to reproduce with consistent properties, thus enabling systematic studies. Previously, we reported on a 3D living-cell-culture tissue-phantom based on 1% agar gel to quantify the physical and biological effects of high-repetition-rate burst-mode laser ablation [18], which suggested that the tensile strength of the phantom can affect characteristic timescales of cavitation in the material, and thereby alter the dynamics of burst-mode absorption. Previous literatures by other authors also showed that cavitation induced by the recoil of ejected material evolved differently in water as compared to in tissue or in tissue phantoms [19–21].

In the present study we irradiated the free surface of pure water as well as hydrogels of different tensile strengths, over a range of irradiances, and determined the dynamic absorption and scattering throughout the pulsetrain, in order to elucidate potential relationships between the tensile strength, laser irradiance, and absorption. From these results, we evaluated the roles that heat diffusion, shock wave propagation, and cavitation dynamics might play in material removal and cellular insult.

## 2. Materials and methods

We described the laser system and the energy partition diagnostic used in this study in a previous work [15]. In brief, the burst-mode ultrafast-pulse laser system uses an Nd: glass flash-pumped and feedback-controlled oscillator that provides 1.5-ps (FWHM) pulses at 1053 nm wavelength. The oscillator pulse-repetition rate is 133 MHz, and the repetition rate of pulsetrain-bursts (shot rate) is 1 Hz. For each shot, the oscillator naturally generates a stable pulsetrain-burst up to 30 µs duration; from these, a Pockels-cell based 'N-pulse selector' can prepare fixed and repeatable selections of burst-duration 100 ns–30 µs. After the desired pulsetrain length is selected, two 4-pass amplifiers amplify the pulsetrain-burst. Amplified per-pulse energy is up to 15 µJ. The amplified pulsetrain-burst is focused onto the target surface in a 5-µm (FWHM) diffraction-limited focal spot, using an aspherical lens (AL2520-B, Thorlabs, USA). In the present study, all targets were irradiated with a single 10-µs long pulsetrain-burst, with the per-pulse irradiance in the order of $10^{12}$ to $10^{13}$ W cm$^{-2}$ [15].

In our preliminary work in hydrogels [18], the plasma self-emission was measured using a 1-ns-risetime photodiode with two short-pass filters (BG39, Schott Glass) to attenuate the reflected 1053-nm laser light at an optical density of ~24. Consistently, the plasma self-emission in the visible-range of the spectrum was observed to last for ~100 ns regardless of pulsetrain-burst duration used down to the minimum achievable burst duration of 0.1 µs, or 10-13 pulses at 133 MHz. Conversely, irradiating solid materials of higher tensile strength (e.g., glass or dental hard tissue) with pulsetrain bursts is seen to result in greater material removal with increasing burst duration [3], and to produce plasma self-emission throughout the entire burst. Importantly, the comparison shows that shielding from the ablation plume is not an explanation: solely the leading 10 to 13 pulses contributed to plasma-mediated ablation of the hydrogel, which can be explained if the first 10 to 13 pulses vaporize sufficient water to explode in a bubble (i.e., explosive boiling), leaving a void on the scale of the Rayleigh range. Indeed, it has been shown elsewhere [22] that bubble formation stops absorption of successive laser pulses and subsequent ablation of water when using fs-laser-pulses, with repetition rates >1MHz.

In our present study, we sought further information by capturing the scattered or reflected light (i.e., non-absorbed energy fraction) of each pulse using a purpose-built energy partition diagnostic based on the double-integrating-sphere principle [15]. Specular reflected, diffuse reflected, and transmitted light were captured in four different integrating cavities, and an absolute calibrated 'incidence energy integrator' measured the incident laser energy. 1-ns

rise-time photodiodes were installed at each integrating cavity, and signals from the photodiodes were recorded by two digital oscilloscopes (TDS 7404, Tektronix, Beaverton, US, and WaveSurfer 454, LeCroy, Chestnut Ridge, US).

Target materials used in this study were distilled water, and agar gel of 1% to 4% agar solid concentration. The targets were ablated at the free surface. Agar gels of different concentrations (1%, 2%, 3% and 4%) were prepared by dissolving agar powder (AGR001.500, BioShop, Burlington, Canada) in distilled water at 80°C. After the agar powder was fully dissolved, the solution was left to cool to 55°C, and then poured onto a glass microscope slide to form a 2-mm-thick gel slab.

A total of 68 shots were fired on distilled water and agar gel targets combined. For each different type of target, data from at least 10 shots were collected.

## 3. Experimental results

Among all the shots recorded, regardless of the target type, the total reflection fractions (Fig. 1) were comparable to the reflection at a water-air interface at low intensity (~3%), and the total reflection fraction showed little variation throughout a pulsetrain (see Fig. 1(b)). The variation in the inferred absorption throughout a pulsetrain came predominantly from the variation in the transmission fraction. As a result, the transmission fraction and the inferred absorption almost mirrored each other.

### 3.1 Characteristics of absorption at the beginning of the pulsetrain

In this part, we consider *the first 200 pulses* of every shot *only*. Absorption dynamics at the beginning of the pulsetrain were characterized by a rapid decrease in transmission, and hence an increase in absorption within the first 20 pulses. For more than 80% of all shots, the global maximum pulse-absorption occurred within the first 20 pulses (150 ns) (Fig. 2(a)). More particularly, 90% of the global maximum absorption was reached within the first eight pulses of a pulsetrain (60 ns) (Fig. 2(b)); virtually all shots reached ≥ 90% of the greatest per-pulse absorption level within the first 16 pulses (120 ns) (Fig. 2(b)).

For irradiances $< 3.0 \times 10^{12}$ W cm$^{-2}$, the peak absorption seen among the first 200 pulses (1.5 μs), absorption was a sensitive function of the irradiance; increasing sharply (Fig. 3(a)). Beyond irradiance $3.0 \times 10^{12}$ W cm$^{-2}$, peak absorption saturated, gradually increasing to ~80% at irradiance $1.5 \times 10^{13}$ W cm$^{-2}$. The type of target (pure water, or hydrogel by concentration) made no noticeable difference. For a comparison, the nominal breakdown thresholds of water are on the order of $10^{11}$ W cm$^{-2}$ for nanosecond pulses, on the order of $10^{11}$ to $10^{12}$ W cm$^{-2}$ for picosecond pulses, and on the order of $10^{12}$ to $10^{13}$ W cm$^{-2}$ for femtosecond pulses [6].

To characterize the absorption during the whole pulsetrain, we first calculated the average absorption per pulse for all the shots (Fig. 3(b)). Similar to Fig. 3(a), average absorption per pulse throughout the whole pulsetrain increased rapidly in the regime $< 3.0 \times 10^{12}$ W cm$^{-2}$. At irradiance $\geq 3.0 \times 10^{12}$ W cm$^{-2}$, however, the average absorption throughout a pulsetrain showed a large variation between shots fired at comparable average irradiance (Fig. 3(b)), and this variation does not particularly depend on agar solid concentration.

The initial rapid increase of absorption at the beginning of the pulsetrain was generally followed by complex fluctuations (see, e.g., Fig. 1(b)). To evaluate the possible contribution of pulsetrain envelope variation in the oscillation of absorption, we calculated the correlation coefficient between the two (Fig. 4(a)), defined by $\dfrac{\sum (X - \overline{X})(Y - \overline{Y})}{\sigma_X \sigma_Y}$. The mean and the standard deviation of all correlation coefficients are –0.1 and 0.3, respectively (see Fig. 4(a)).

There was variation of laser irradiance, within the pulsetrain envelopes, resulting from the active feedback-stabilization within the oscillator. These variations of intensities within each

pulsetrain were characterized using the coefficient of variation (the ratio of standard deviation and the mean), and were within 13% (Fig. 4(b)).

## 3.2 Periodicity of oscillations in absorption patterns

The pronounced fluctuations in absorption, on timescales of roughly 1−3 µs, were analyzed to identify any periodicity, any regular oscillation. Such oscillation could result, for instance, if a cavitation bubble were to be created with the initial breakdown: the range of expansion and collapse of a cavitation bubble could be significant compared to the Rayleigh range of the focus (~50 µm) and therefore absorption would fluctuate according to whether the laser was focused into the cavity void or collapsing solid.

To characterize any patterns of oscillation in the absorption, we calculated the autocorrelation of the time-dependent absorption (e.g., Fig. 5(a)) for bursts at $I \geq 3.0 \times 10^{12}$ W cm$^{-2}$, when peak absorption saturated, and absorption behavior was most reproducible. The autocorrelation trace makes apparent a longer-time order in the absorption, a recurrence that suggests 'ringing'. The recurrence time provides a measure of the periodicity in the absorption pattern, and the recurrence amplitude characterizes the coherence of the oscillation (Fig. 5(a)). From such traces, we calculated mean periods for all shots that showed definite ringing, defined as more than three recurrences, with the minimum 0.5-µs time separation between recurrences (11 out of 68 shots) (Fig. 5(b)). Notably, these multiple bounces appear only in the higher-tensile strength hydrogels — none of the distilled water or 1% agar gel shots show three or more periods of oscillation within the 10-µs recording length. However, there is no clear distinction between 2% to 4% agar gels in their periods of oscillation. A recording length longer than the 10-µs used in the present study is required for studying the oscillations in weaker targets such as distilled water, and 1% agar gel.
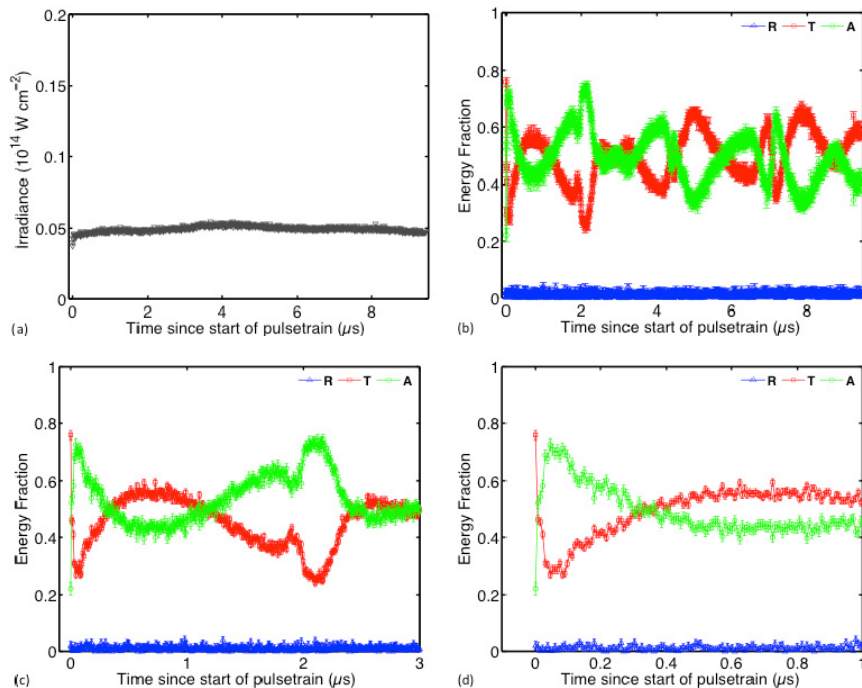


Fig. 1. Burst-mode irradiation of a 4% agar gel (single 10-µs burst, 133-MHz pulse repetition-rate, $I_{avg} = 5.0 \times 10^{12}$ W cm$^{-2}$. A total of 1,250 pulses were recorded, limited by the record-length of the oscilloscope: (a) Input pulsetrain envelope. (b) The time-resolved total reflection ($R$), transmission ($T$), and net absorption ($A$). (c) and (d) each shows the first 3 µs and 1 µs of subplot (a), respectively.
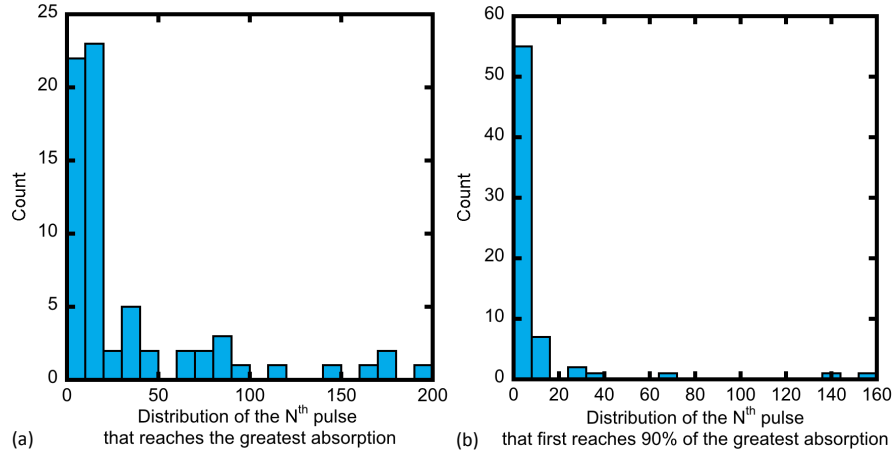
Fig. 2. Considering only the first 200 pulses: (a) distribution by pulse number *N of* which pulse in the burst experiences the greatest absorption, (b) distribution by pulse number *N* of which laser pulse first surpasses 90% of the peak absorption.
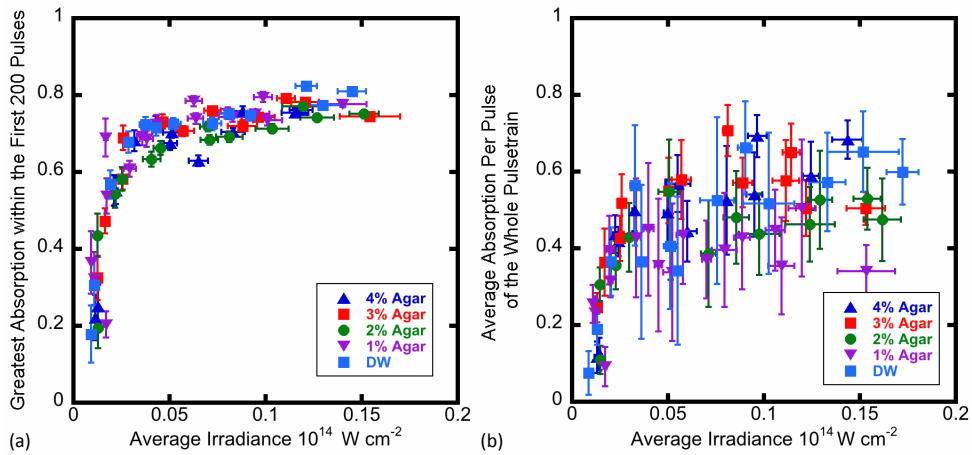


Fig. 3. Absorption of first 200 pulses in the burst (a) Peak *per-pulse* absorption fraction vs. irradiance (b) Average per-pulse absorption vs. irradiance. (all samples: distilled water and agar gels of different concentrations; single 10-µs burst, 133-MHz pulsetrain.) The per-pulse peak absorption reflects optical breakdown physics; the per-pulse averaged absorption reflects optical breakdown combined with subsequent ionization dynamics and hydrodynamics.
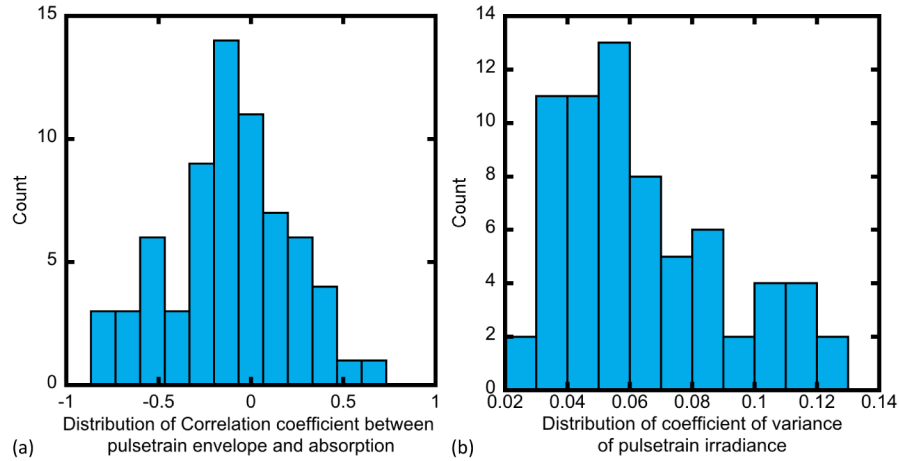
Fig. 4. (a) the distribution of coefficients of correlation comparing the intensity of incident pulses and their absorption, for 68 separate burst-shots. The mean and the standard deviation of all correlation coefficients are $-0.1 \pm 0.3$. (b) stability of input pulsetrain-bursts, from the distribution of coefficients of variance of pulse irradiances. The coefficient of variance is calculated as the ratio between the standard deviation and the mean of the pulsetrain irradiance.
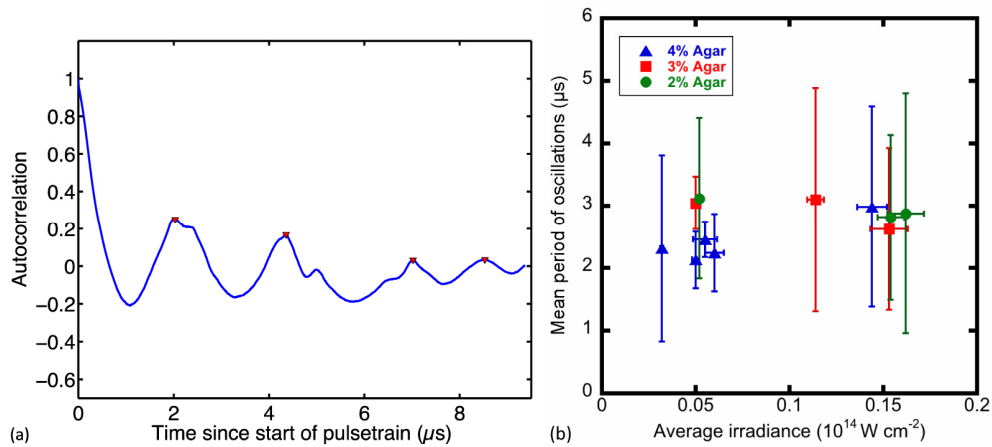


Fig. 5. (a) Autocorrelation of the time-dependent absorption corresponding to Fig. 1(b). (b) Mean periods of oscillation, identified from the autocorrelation of absorption, for shots with $I_{avg} \geq 3.0 \times 10^{12}$ W cm$^{-2}$ and which exhibited three or more cycles of oscillation.

## 4. Discussion

### 4.1 Ablation dynamics

It is well-recognized, in intense optical physics with solid dielectrics, that the optical breakdown threshold for surface irradiation is typically less than that within the bulk [23]. This is generally considered to result from surface defects — microfields are enhanced, where the fissures or scratches resulting from surface polishing, for example. In the case of free surfaces of liquids, the differences and distinctions are less clear, and experimental results are mixed. Following initial optical breakdown, marked in our studies by a very abrupt drop in transmission owing to an overdense plasma created at the interface, all components of scattered light remain low — specular reflection, broader backscatter and side-scatter included (Fig. 1). The observed increase in absorption may be due to several factors:

1) Though much heat leaves with ablated material in such short-pulse irradiation, heat is recognized to accumulate during burst-mode irradiation [3], and this has the potential to alter the linear absorption coefficient of the material [24].

2) Ionization created by a pulse does not fully recombine during the 7.5ns interval between pulses. Docchio [7] found a low nanosecond-timescale exponential tail for recombination, and so ionization does not need to re-initiate with each new pulse. Thus plasma-mediated ablation is 'simmered' or kept alive at low levels from pulse to pulse during our 133-MHz pulsetrain burst.

3) Plasma self-emission in visible and near-infrared light begins with optical breakdown and lasts only for ~100 ns in these hydrogels, as compared to throughout the whole burst train in glass and metals. This can only arise if there is little matter present over multiple Rayleigh ranges around the focal region, which includes the whole extent of the ablation plume formed over this timescale. This argues for the formation of a void. Coincident with this, the transmission of laser light through the target increases again almost to original levels and absorption drops greatly. With low measured scatter, clearly any ablation plume plays a negligible role in dynamics at this point. On this point, the role of the impact of ablation plume in ultra-high-repetition-rate burst-mode processing, we note that the recent development of GHz burst-mode fiber lasers [25] has permitted ablation in soft and hard tissues up to 3 mm³/min average rates, an order of magnitude higher than previously reported [26]. Ablation plume dynamics in high-ablation-rate processing is not automatically an impediment.

The later recurrence of absorption evidences that the material void closes after a few microseconds (Fig. 1 (b)), when not being actively driven by the laser. It appears the laser pulse-train drives open a void, from which point there is no further absorption and no further heating, therefore the void closes again, only then to then intercept the focal spot once more, and the process repeats. Single images we have recorded in prior experiments suggest that this void may happen along a filament penetrating a few Rayleigh-ranges into the hydrogel, but we cannot image while simultaneously time-resolving the energy-partitioning in our integrating-sphere-based device. Therefore we cannot definitively establish the geometry of the void created: it may be direct cavitation within the bulk hydrogel or it may be recoil of the free surface, driven by hot vapour expanding which drives a bubble inward, either entrapping the vapour before collapsing or else expelling it before restoring the surface.

Figure 3(a) implies that the absorption at the beginning of the pulsetrain depends on the previous pulse's irradiance, reflecting the nonlinear nature of plasma-mediated absorption. The modest variations from shot-to-shot in the absorption, averaged over the whole burst at comparable laser irradiance (Fig. 3(b)), could result from variations between the pulsetrain envelopes. However, the correlation found between pulsetrain envelopes and corresponding absorption histories is very weak — and negative rather than positive (Fig. 4(a)).

The bouncing of cavitation bubbles generated by a single laser pulse within bulk water [27] and within bulk hydrogel [28] was previously observed by other authors. These studies showed experimentally that the cavitation bubble oscillated within the bulk material, with the maximum radius of the bubble decreasing in every cycle of the oscillation [27,28].

Most simply, within bulk water, the relation between maximum radius of a spherical cavitation bubble and its oscillation period $T_B$ can be described by the Rayleigh model [14,29]:

$$T_B = R_{max} \left( 2 \times 0.915 \sqrt{\frac{\rho_0}{\rho_0 - \rho_v}} \right). \tag{1}$$

where $R_{max}$ is the maximum radius of the bubble, $\rho_0$ is the density of water, $p_0$ is the hydrostatic pressure, and $p_v$ is the vapor pressure inside the bubble [14]. The Rayleigh model assumes that the liquid is incompressible, and it neglects viscosity and surface tension [29]. According to the Rayleigh model, the oscillating period of a 100-μm radius cavitation bubble in water is about 18 μs. For the cavitation bubbles inside agar gels, one would expect the oscillation period would be shorter due to the higher tensile strength compared to distilled water [28]. While previous authors used more sophisticated numerical model, such as the Rayleigh-Plesset model [27], to explain the dynamics of cavitation bubble oscillation within bulk material, it should be noted that such model may not apply to the cavitation bubble near a free surface. It is reasonable to expect the collapse of the cavitation bubbles in this study to be asymmetric because the bubbles are adjacent to the water-air interface. The collapse of a cavitation bubble near a boundary typically results in the formation of a jet [30,31]. Thus, future experiments to fully elucidate the mechanism of burst-mode tissue ablation require shadowgraphy, Koehler illumination, or Schlieren photography to provide more details about geometry, and the evolution of any cavitation bubble in relation to its pressure $p_v$.

### 4.2 Mechanisms in material removal and cellular death

Vogel *et al.* [14] measured how energy absorbed from a laser pulse is ultimately partitioned over bulk heat, latent heat of phase changes material flow, cavitation and shock waves, following breakdown within bulk water, using single ultrafast pulses of different pulse widths and pulse energies. For conditions closest to ours, Vogel found that when a 30-ps, 50-μJ pulse induced optical breakdown in water, 59% of the pulse energy is absorbed. Out of this absorbed energy, an induced shock wave accounted for 10% to 23%, and a cavitation bubble for 11% of this total available energy. Vaporization accounted for 16%, however 15% of the absorbed energy ultimately went unattributed [14]. We assume that roughly the same energy partition between different physics mechanisms applies to our experiment, except that the cavitation bubble energy found in Vogel's work will in our case appear as the kinetic energy coupled into both substrate and the ejected material, since ablation in this work began at the material free surface. The total kinetic energy then accounted for ~19% of absorbed energy. Since the net momentum of ejected material and substrate material, together, must be zero, and since the mass of ejected material was much smaller than the substrate, we expect most of this kinetic energy went to the kinetic energy of ejected material. For laser energies ~10 μJ per pulse, we previously determined that the ablated volume in a 1% agar gel is on the order of $10^{-3}$ mm$^3$ [18]. We further assume 70% average absorption for the first 10 pulses that accounted for most of material removal, the average speed of the $10^{-3}$ mm$^3$ of ejected material would be up to 170 m s$^{-1}$. In comparison, completely vaporizing $10^{-3}$ mm$^3$ of 1% agar gel at 20°C requires 2.6 mJ of energy, which exceeds the total energy of the entire pulsetrain. Although vaporization plays an essential role in driving material ejection, it cannot be the sole way in which material is removed; much of the removed material will leave as disintegrated fragments.

In Vogel's work [14], the shock wave accounted for up to ~40% of absorbed energy. To estimate the shock wave pressure, we consider the case where a water or agar gel target was irradiated with a single pulsetrain-burst with a flat pulsetrain envelope, and 10 μJ pulse energy. Assuming that absorption reached ~70% for the early pulses of the pulsetrain (estimated from Fig. 3(a)), then the strongest shock wave generated by the single pulse with highest peak absorption can contain ~2.8 μJ energy. We further assume that pulse will generate a spherical shock wave with an exponential pressure temporal profile [32,33]:

$$p(t) = p_s \cdot \exp\{-t/t_0\}, \tag{2}$$

where $t$ is the time past the peak shock pressure, and $t_0$ is is the characteristic time for shock pressure to decay to *1/e* of the peak pressure $p_s$, and this peak pressure is expected to

decrease as the shockwave propagate further away from the origin. The energy $E_S$ contained in a spherical shock wave is [32,33],

$$E_S = \frac{4\pi R^2}{\rho_0 c_0} p_S^2 \cdot \frac{t_0}{2}, \qquad (3)$$

where $\rho_0, c_0$ are the density and sound speed in water, $R$ is the distance from the irradiation spot. For $t_0$, we adopt the value estimated by Vogel et al. using the Gilmore model, a 30-ps, 50-µJ pulse-induced shock wave within bulk water is 20 ns [33]. It is estimated [29] that 50–100 MPa of shock wave pressure is likely to result in cellular damage. From Equation. 3, one can obtain an upper bound for the range of shock wave damage. Assuming a 2.8 µJ shock wave propagating without dissipation in agar gel or water, the range over which 50-MPa peak shock pressure is exceeded would be less than 110 µm, and the damage range associated with 100-MPa threshold peak shock pressure would be smaller than 60 µm. This damage range appears to be comparable to the cellular necrosis range we previously measured in the 1% agar gel tissue phantom under similar laser conditions [18]; based on our current assessment of absorption dynamics, shockwave damage is a probable cause of cellular necrosis in our earlier work.

## 5. Conclusion

In summary, dynamic measurements of absorption and scattering of 10-µs bursts of 1.5-ps laser pulses at 133 MHz repetition rate, in in hydrogel targets, have found absorption to rapidly increase at the beginning of each pulsetrain burst. In over 80% of the shots in this series, greatest absorption was found within the first 20 pulses. This strong initial absorption was followed by few-microsecond oscillations in the absorption fraction, with no correlation to intensity changes in the pulsetrain envelope; this oscillation and its timescale point to hydrodynamics driven in the hydrogel. Very probably, these oscillations result from a cavitation bubble created at laser focus by the early pulses, from strong recoil of the ablated surface or from penetration of the laser ~50-100µm over the Rayleigh range into the bulk, which subsequently collapses, only to again be driven by new absorption. The timescale for oscillations showed only weak dependence on tensile strength of the hydrogel, ranging from distilled water to 4% agar concentration.

Based on quantitative energy absorption, for burst-mode ultrafast ablation of agar hydrogels, vaporization cannot be the principal mechanism of surface ablation, though vaporization-driven cavitation bubbles are likely responsible for ablation by disintegration. Also based on quantitative dynamics, the associated shock wave has sufficient strength to explain our earlier *in vivo* observations of the range of cellular necrosis in regions of tissue-phantom lying intact beyond the ablation crater.